Photochemical formation of the ultrafine aerosol in the atmosphere over a continental region

M.Yu. Arshinov, B.D. Belan, and D.V. Simonenkov

Institute of Atmospheric Optics,
Siberian Branch of the Russian Academy of Sciences, Tomsk

Received December 22, 2005

Monitoring of ultrafine particles renewed in 2005 confirmed the presence of a clearly bell-shaped diurnal behavior of their concentration. An estimate of the rate of new particle formation due to gas-to-particle conversion has been performed based on the diurnal behavior of nanoparticle concentration. Concentrations of the major aerosol precursors have been calculated. Rough estimate of nanoparticle growth rate has been done.

Introduction

Global warming is a heated issue of public discussions today, both in science and politics/economics, with the primary concern in the greenhouse gases while the atmospheric aerosol stands in the second place. The role of aerosol is as a rule considered from the viewpoint of its possible contribution to climatic changes, directly through its scattering and absorption of solar radiation and indirectly through cloud formation. However, these processes mostly involve large particles, more than 0.1 μm in size. By now, these particles as well as the processes of their formation and transformation have been well investigated.

A series of climate models have appeared recently that take into account the role of aerosol in climate changes. However, no clear understanding of the effects of aerosol chemical composition on its scattering and absorbing properties have been formed up to now, for the available methods of chemical analysis of aerosol samples allow us to get the information about their ionic and elemental composition rather than about the particulate matter itself.

With the advent of reliable modern experimental methods and theoretical basis, rapidly growing number of studies deals with the aerosol of nanometer size range, which hold the major amount of the atmospheric particles (the number concentration is meant here). Despite all the success achieved, determination of the chemical composition of ultrafine particles and the so-called Aitken nuclei remains one of the most difficult problems, which complicates elucidation of the processes governing the aerosol formation from the gas phase in the atmosphere.[1] Since the present-day technologies yet do not allow us to determine neither the size of critical embryos nor their chemical or elemental composition indirect search for the most probable processes using the available means, including *in situ* measurements of nanoparticles and gas precursors of aerosol and the laboratory experiments is perhaps the only way to solve this problem.

In building up a model, one should take into account, besides the role of aerosol, photochemical processes that yield its formation because these determine the physicochemical properties of the particles formed, their transformations, and formation of the aerosol and cloud fields in the atmosphere. Note that the photochemical reactions giving rise to formation the vapor of the aerosol-forming compounds (VAFC) often involve some greenhouse gases. Search for the main photochemical processes yielding formation of new particles is a difficult task. There are many photochemical reactions that simultaneously occur in the atmosphere, but not all of them result in a gas-to-particle conversion. There are only a small number of reactions yielding aerosol *in situ* and, consequently, determining the intensity of this process, because the rate of these reactions is a limiting factor in the VAFC generation. If we regard aerosol formation as a continuous process,[2] then formation of aerosol particle from gas phase is its beginning. It should not be too complicated, for we know that the more complex the system the less stable it is. Therefore, in this case, the probability of forming stable embryos is low. Besides, the process of new particle formation strongly depends on the intensity of the incoming solar radiation.[3,4]

1. Photochemical reactions yielding aerosol *in situ*

From the theory of aerosol formation from the gas phase (hereafter: nucleation) we know that stable embryos or clusters appear mostly as a result of

– binary heteromolecular nucleation of sulfuric acid and water;

– a three-component nucleation of sulfuric acid, water, and ammonia;

– a binary nucleation of nitric acid and water.

0235-6880/06/04 292-12 $02.00

In its turn, the appearance of the molecules of sulfuric and nitric acids in a clean atmosphere is the result of a chain of photochemical and catalytic reactions that involve sulfur dioxide and nitrogen and ozone oxides. In this section, we briefly analyze only those reactions, which can occur under real conditions in the troposphere.

1.1. Reactions involving sulfur-containing compounds

All the major gas-phase reactions leading to formation of sulfuric acid are, first of all, connected with the primary oxidation of SO_2 to SO_3. Formation of SO_3 can occur under a direct photochemical oxidation of sulfur dioxide in the following chain of reactions[4,5]:

$$SO_2 + h\nu \rightarrow SO_2^* \text{ excited state } (^1SO_2), \quad (1)$$

$$^1SO_2 + M \rightarrow {}^3SO_2 - \text{singlet-triplet conversion}, \quad (2)$$

$$^3SO_2 + SO_2 \rightarrow SO + SO_3, \quad (3)$$

$$SO + O_2 \rightarrow SO_3. \quad (4)$$

The rate of this complex conversion depends mainly on the rates of reactions (2)–(4) and generally, it is not high. This mechanism is efficient rather for the upper troposphere and the lower stratosphere and not in the atmospheric boundary layer (Ref. 5).

Table 1 gives the kinetic characteristics of SO_2 oxidation reactions by the main atmospheric oxidizers: ozone, oxygen, the radicals $OH^\bullet$ and $CH_3O_2^\bullet$ and the hyperoxyde radical $HO_2^\bullet$ (Refs. 6–9).

From the data given in Table 1 we can see that a gas-phase conversion of sulfur dioxide occurs mainly in the reactions with radicals. Here, the most probable reaction is the reaction with the hydroxyl radical (5), whose rate is 2 to 3 orders of magnitude higher than the rates of other reactions. The final conversion yielding the molecules of H_2SO_4 is represented by the chain (11). Reaction (7) can significantly contribute to SO_2 oxidation only in the stratosphere.[6]

1.2. Reactions involving nitrocompounds

Before considering formation of nitric acid in the atmosphere, we would like to say some words about the role of nitrogen oxides in the formation of sulfuric acid. According to V.A. Isidorov,[6] the laboratory experiments in smog chambers showed that the rate of sulfur dioxide oxidation can strongly increase in the presence of nitrogen oxides. This process can be described as follows:

$$SO_2 + OH^\bullet \rightarrow HSO_3^\bullet, \quad (12)$$

$$HSO_3^\bullet + O_2 \rightarrow HSO_5^\bullet, \quad (13)$$

$$HSO_5^\bullet + NO \rightarrow HSO_4^\bullet + NO_2, \quad (14)$$

$$HSO_4^\bullet + NO_2 + H_2O \rightarrow H_2SO_4 + HNO_3. \quad (15)$$

The result of these processes can be the products of both sulfuric and nitric acids.

The analysis of the rates of kinetic and photochemical reactions including the latest data recommended by the subcommittee estimating the gas-kinetic data of the atmospheric chemistry of the International Union of Pure and Applied Chemistry (IUPAC) proves that the main role in the gas-phase reactions of nitrogen oxide oxidation belongs to those that involve various radicals (Table 2).

Thus, from the data on the reaction rate (see Sects. 1.1 and 1.2) we see that the key substances taking part in formation of the VAFC field, which are then converted to the aerosol phase, are radicals (mostly, the hydroxyl radical). However, the rate of the reactions yielding the nitrogen acid molecules is an order of magnitude higher than the rate of reactions yielding sulfuric acid.

Table 1. The constants of gas-phase oxidation reactions of sulfur oxides (k, $cm^3/(s \cdot mol.)$)

Reaction	k (Ref. 6)	k (Ref. 7)	k (Ref. 9)	k (Ref. 8)	No.
$SO_2 + OH^\bullet \rightarrow HOSO_2^\bullet$	–	$1.3 \cdot 10^{-12}$	$1.5 \cdot 10^{-12}$	$1.3 \cdot 10^{-12}$	(5)
$SO_2 + HO_2^\bullet \rightarrow SO_3 + OH^\bullet$	$7.8 \cdot 10^{-16}$	$1.0 \cdot 10^{-15}$	–	$<1.0 \cdot 10^{-18}$	(6)
$SO_2 + O^\bullet + M \rightarrow SO_3 + M$	–	$1.0 \cdot 10^{-14}$	–	–	(7)
$SO_2 + CH_3O_2^\bullet \rightarrow SO_3 + CH_3O$	$1.8 \cdot 10^{-14}$	$3.3 \cdot 10^{-15}$	–	–	(8)
$SO_2 + O_3 \rightarrow SO_3 + O_2$	$1.0 \cdot 10^{-22}$	$1.0 \cdot 10^{-22}$		–	(9)
$SO_2 + O_2 \rightarrow SO_3 + O^\bullet$	$1.0 \cdot 10^{-30}$	$1.0 \cdot 10^{-30}$			(10)
$SO_2 + OH^\bullet \rightarrow HOSO_2^\bullet$		$1.3 \cdot 10^{-12}$	$1.5 \cdot 10^{-12}$	$1.3 \cdot 10^{-12}$	
$HOSO_2^\bullet + O_2 \rightarrow HO_2^\bullet + SO_3$	$1.8 \cdot 10^{-12}$	–	$1.3 \cdot 10^{-12}$	–	(11)
$SO_3 + H_2O + M \rightarrow H_2SO_4 + M$	(for the whole chain)	$1.0 \cdot 10^{-12}$		$5.7 \cdot 10^4$ s^{-1} (at a 50% rel. humid.)	

Table 2. The constants of gas-phase oxidation reactions of nitrogen oxides (k, $cm^3/(s \cdot mol.)$)

Reaction	k (Ref. 6)	k (Ref. 7)	k (Ref. 9)	k (Ref. 8)	No.
$NO + O_3 \rightarrow NO_2 + O_2$	–	$1.6 \cdot 10^{-14}$	$1.8 \cdot 10^{-14}$	$1.8 \cdot 10^{-14}$	(16)
$NO_2 \xrightarrow{h\nu} NO + O(^3P)$, $\lambda < 398$ nm	–	$4.0 \cdot 10^{-3}$	–	301 kJ·mole^{-1}	(17)
$NO_2 \xrightarrow{h\nu} NO + O(^1D)$, $\lambda < 244$ nm	–			490 kJ·mole^{-1}	
$NO + HO_2^{\bullet} \rightarrow NO_2 + OH^{\bullet}$	$2.4 \cdot 10^{-11}$	$8.1 \cdot 10^{-12}$	–	$8.8 \cdot 10^{-12}$	(18)
$NO_2 + O_3 \rightarrow NO_3 + O_2$	$1.2 \cdot 10^{-13} \exp[-2450/T]$	$1.3 \cdot 10^{-17}$	$3.2 \cdot 10^{-17}$	$3.5 \cdot 10^{-17}$	(19)
$NO_3 + NO \rightarrow NO_2 + NO_2$	–	$1.9 \cdot 10^{-11}$	$2.6 \cdot 10^{-11}$	$2.6 \cdot 10^{-11}$	(20)
$NO_3 \xrightarrow{h\nu} NO_2 + O(^3P)$, $\lambda < 587$ nm	–	$2.1 \cdot 10^{-1}$	–	204 kJ·mole^{-1}	(21)
$NO_3 \xrightarrow{h\nu} NO + O_2(^3\Sigma)$, $\lambda < 11080$ nm	–	$8.3 \cdot 10^{-2}$	–	10.8 kJ·mole^{-1}	(22)
$NO_3 \xrightarrow{h\nu} NO + O_2(^1\Delta)$, $\lambda < 1139$ nm				105 kJ·mole^{-1}	
$NO_3 \xrightarrow{h\nu} NO + O_2(^1\Sigma)$, $\lambda < 714$ nm				168 kJ·mole^{-1}	
$NO_2 + OH^{\bullet} + M \rightarrow HNO_3 + M$	$1.1 \cdot 10^{-11}$	$9.0 \cdot 10^{-12}$	$2.4 \cdot 10^{-11}$	$4.1 \cdot 10^{-11}$	(23)
$3NO_2 + H_2O \rightarrow 2HNO_3 + NO$	–	$2.0 \cdot 10^{-25}$	–	–	(24)
$NO_3 + NO_2 + M \rightarrow N_2O_5 + M$	$1.48 \cdot 10^{-13} \exp[861/T]$	–	$1.5 \cdot 10^{-12}$	$1.9 \cdot 10^{-12}$	(25)
$N_2O_5 + H_2O \rightarrow 2HNO_3$	–	–	–	$2.5 \cdot 10^{-22}$	(26)
$NO + CH_3O_2^{\bullet} \rightarrow NO_2 + CH_3O$	$1.7 \cdot 10^{-11}$		–		(27)
$NO_2 + RCOOO \rightarrow RCOOONO_2$	–	$1.4 \cdot 10^{-15}$	–	–	(28)

Thus, we have established that the presence of radicals restricts the rate of the VAFC formation. So, below we consider the constants of the radical formation rates.

1.3. Formation of radicals in the atmosphere

The hydroxyl radical can form in a direct photolysis of water vapor. However, this reaction needs hard radiation with the wavelengths shorter than 242 nm. Hence, it is possible only in the upper atmospheric layers. According to V.A. Isidorov,[6] the main source of hydroxyl radicals is the reaction of water molecules with a metastable oxygen $O(^1D)$. And the main source of $O(^1D)$ in the troposphere is the ozone photolysis (see Table 3).

V.A. Isidorov, having summarized the data on the rates of the reactions related to formation and sink of hydroxyl radical, suggested the following equations for calculating the stationary concentration of a metastable oxygen and hydroxyl radical[6]:

$$[O(^1D)] = \frac{J_{29}[O_3]}{k_{32}[M] + k_{30}[H_2O] + k_{31}[H_2O]}; \quad (37)$$

the photodissociation coefficient is

$$J = \int_0^{\infty} \varphi_\lambda \sigma_\lambda I_\lambda d\lambda, \quad (38)$$

where φ_λ is the quantum yield of O_3 dissociation under absorption of light with the wavelength λ; σ_λ is the absorption cross section of the ozone molecule for light at the wavelength λ; I_λ is the quantum flux rate, quantum·$cm^{-2} \cdot s^{-1}$;

$$[OH^{\bullet}] = \frac{2k_{30}[O(^1D)][H_2O]}{k_{33}[CO] + k_{34}[CH_4] + k_{35}[O_3]}. \quad (39)$$

Now, having known the density of 320 nm UV flux, we can roughly calculate the concentration of hydroxyl radical using Eqs. (37)–(39).

Table 3. Main radical yielding reactions (k, $cm^3/(s \cdot mol.)$)

Reaction	k (Ref. 6)	k (Ref. 7)	k (Ref. 9)	k (Ref. 8)	No.
$O_3 \xrightarrow{h\nu} O_2(^1\Delta_g) + O(^1D)$, $\lambda < 310$ nm	–	$2.6 \cdot 10^{-5}$ s^{-1}	–	386 kJ·mole^{-1}	(29)
$O(^1D) + H_2O \rightarrow 2OH^{\bullet}$	$2.2 \cdot 10^{-10}$	$2.3 \cdot 10^{-10}$	–	$2.2 \cdot 10^{-10}$	(30)
$O(^1D) + H_2O \rightarrow O(^3P) + H_2O^*$	$2.9 \cdot 10^{-11}$				(31)
$O(^1D) + M \rightarrow O(^3P) + M^*$	$2.9 \cdot 10^{-11}$	$2.9 \cdot 10^{-11}$	–	–	(32)
$CO + OH^{\bullet} \rightarrow CO_2 + H^{\bullet}$	–	–	$1.5 \cdot 10^{-13}$	–	(33)
$CH_4 + OH^{\bullet} \rightarrow CH_3 + H_2O$	$8.0 \cdot 10^{-15}$	–	$6.3 \cdot 10^{-15}$	–	(34)
$O_3 + OH^{\bullet} \rightarrow HO_2^{\bullet} + O_2$	–	$5.2 \cdot 10^{-14}$	$6.8 \cdot 10^{-14}$	$7.3 \cdot 10^{-14}$	(35)
$O_3 + HO_2^{\bullet} \rightarrow OH^{\bullet} + 2O_2$	$2.0 \cdot 10^{-15}$	$2.0 \cdot 10^{-15}$	$2.0 \cdot 10^{-15}$	$2.0 \cdot 10^{-15}$	(36)

2. Instrumentation

In our experiments, we have used the datasets of atmospheric parameters measured at TOR Station of the IAO SB RAS. The measurement instrumentation complex of the Station consists of the four main blocks: meteorological, aerosol, gas, and the radiation one.[10]

The concentration and size-distribution of 3 to 200-nm sized particles were recorded with an 8-channel automated diffusion battery (ADB). The time needed to completely scan all the channels and to reconstruct the full spectral range is six minutes. Our ADB is a new version of a diffusion aerosol spectrometer (DAS).[11] Its main distinction from the traditional DAS is a new electronics interface that provides for a higher stability and reliability of the device operation, which is important in a non-stop long-term monitoring. The DAS block of the diffusion battery, the condensation coagulator, and the photoelectron particle counter themselves, has remained unchanged. To transform the data on particle slippage into the size distribution data, we traditionally used the Ankilov–Eremenko algorithm, which was recognized as the best one and has for a long time been used by the TSI Company for their diffusion batteries.[12]

Gas concentrations were measured with chemiluminescent gas analyzers: dioxide with an S-310, nitrogen monoxide and dioxide with an R-310, and ozone with a 3.02P devices.

The lower detection limit of all the three gas analyzers is about 1 $\mu g/m^3$.

Continuous measurements of the integral intensity of the UV-B radiation within the region of 280–320 nm were performed with a UVB-1 pyranometer (Yankee Environmental Systems, Inc., USA). With the Brewer spectrophotometer we have performed occasional measurements of the UV radiation intensity in the region from 290 to 325 nm with a step of 0.5 nm.

3. Results and discussion

Yet in 1996, a continuous monitoring of ultrafine aerosol has revealed a distinct diurnal behavior of the concentration of aerosol particles with the sizes below 10 nm in diameter exhibiting a daytime maximum, which proves prevalence of photochemical processes in the formation of these particles.[3] However, at that time, our instrumentation did not allow us to check it *in situ*, what processes occur in the atmosphere. In the meantime, we already knew that there exists a relation between the dynamics of the ozone concentration and ultrafine particles ($d_p < 10$ nm), namely, that ozone generation is often synchronous with nanoparticle formation.[13] In spite of the extension of the TOR Station capabilities that took place in recent years, it still could not cover the entire nomenclature of the desired parameters. Nonetheless, it helps in estimating the rates of the most probable processes that lead to phase transformation of the atmospheric matter.

3.1. Diurnal variation of the ultrafine particle concentration

In March, 2005 we have resumed the monitoring of ultrafine aerosol at the TOR Station, which showed again the presence of a steady bell-shaped diurnal variation of the ultrafine particle concentrations (Fig. 1), irrespective of the season. Hence, this regularity must be determined by some parameter or a process.

The relation between the solar radiation intensity and aerosol particle formation is considered in Ref. 3. However, in that work we have just established this fact, having at our disposal only the data on the total solar radiation in the region from 0.4 to 2.3 μm. This circumstance did not allow us to perform any precise calculations. The above analysis of photochemical reactions suggests that the most intense processes occur under the action of hard UV radiation with the wavelengths below 320 nm. However, this relation is indirect, for the solar radiation itself cannot directly synthesize solid or liquid phase particles in the atmosphere. At the same time, it plays a decisive role in the formation of the field of aerosol-precursor gases.

3.2. Calculation of hydroxyl radical concentration

Thus, we have found that formation of aerosol from the gas phase is governed first of all by the hydroxyl radicals. Direct OH measurements show that a rapid growth and decay in the radical concentration coincide with the sunrise and sunset time,[14] and its diurnal variation is bell-shaped too. This fact has allowed R. Weber[14] to infer that this variation follows from the variations of the UV radiation.

Thus, if we know the UV radiation intensity, we can quite accurately calculate the concentration of hydroxyl radical by Eqs. (37)–(39).

To calculate the $O(^1D)$ and OH concentrations by Eqs. (37)–(39), we have all data we need: O_3, CO, and atmospheric gases M concentrations (reference information); the concentration of water molecules can be calculated from the relative humidity by the equation

$$[H_2O] = 6.1078 \cdot 10^{\frac{7.665t}{243.33+t}} \frac{217f}{(273.15+t)} \frac{N_A}{M_{H_2O}} \cdot 10^{-6}, \quad (40)$$

where f is the relative humidity in fractions of unity; t stands for the temperature °C; N_A is the Avogadro constant; M_{H_2O} is the molecular weight of water.

For the methane concentration, we took its average values normal for our region. These values were calculated by using data of monitoring over Siberia under the joint Russian–Japanese project on studying greenhouse gases.

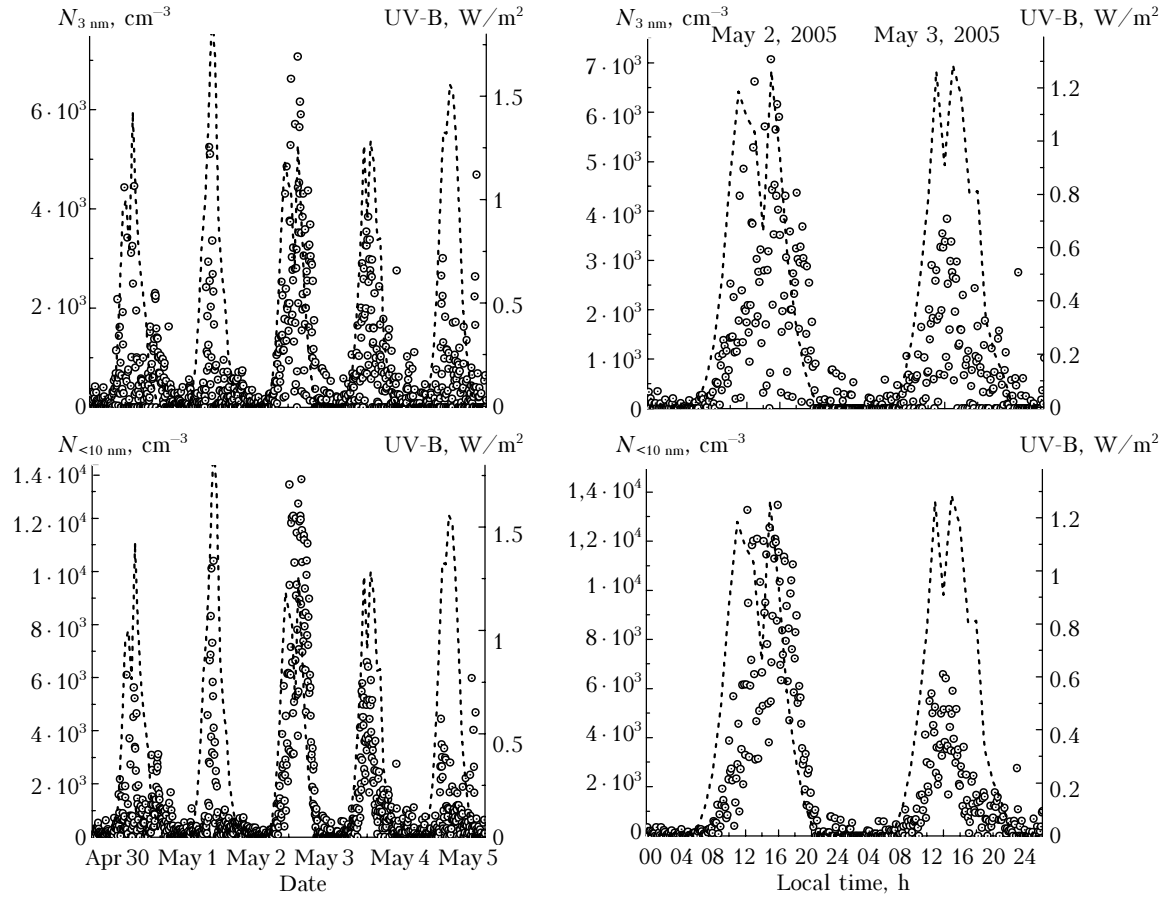

Fig. 1. Temporal behavior of nanoparticle concentration and integral intensity of UV-B radiation in a region 280–320 nm.

In the calculation of the ozone photodissociation coefficient J we used the data recommended by R. Atkinson et al.[8] The quantum yield $\varphi[O(^1D)]$ at $\lambda < 305$ nm is 0.9 and does not depend on temperature. For $306 < \lambda < 320$ nm the quantum yield was calculated by the following equation[8]:

$$\varphi(\lambda,T) = \left\{\frac{q_1}{q_1+q_2}\right\} A_1 \exp\left\{-\left(\frac{X_1-\lambda}{\omega_1}\right)^4\right\} +$$

$$+\left\{\frac{q_2}{q_1+q_2}\right\} A_2 \left\{\frac{T}{300}\right\}^2 \exp\left\{-\left(\frac{X_2-\lambda}{\omega_2}\right)^2\right\} +$$

$$+A_3\left\{\frac{T}{300}\right\}^{1.5} \exp\left\{-\left(\frac{X_3-\lambda}{\omega_3}\right)^2\right\} + c_1, \qquad (41)$$

where λ is the wavelength, nm; $q_i = \exp[-\nu_i/(kT)]$; $A_1 = 0.8036$; $A_2 = 8.9061$; $A_3 = 0.1192$; $X_1 = 304.225$; $X_2 = 314.957$; $X_3 = 310.737$; $\omega_1 = 5.576$; $\omega_2 = 6.601$; $\omega_3 = 2.187$; $\nu_1 = 0$; $\nu_2 = 825.518$; $c_1 = 0.0765$; $k = 0.695$.

Though at the wavelengths longer than 305 nm the quantum yield sharply decreases down to ≈ 0.1 at $\lambda = 320$ nm, we must still take it into account while calculating J, because the intensity of the quantum flux near the earth's surface in the considered wavelength region is several times larger than in the region below 305 nm.

The quantum flux rate is calculated by the equation

$$I_\lambda = \lambda Q_\lambda/(hc), \qquad (42)$$

where Q_λ is the solar radiation intensity at the wavelength λ (W·cm^{-2} or J·s^{-1}·cm^{-2}); h is the Planck's constant; c is the speed of light.

The values of the ozone absorption cross section in the wavelength region of interest are listed in Table 4.

Table 4. Ozone absorption cross section,[8] JPL NASA-14

λ, nm	$\sigma\cdot10^{20}$, cm^2 (T = 273 K)
281.7	402
285.7	277
289.9	179
294.1	109
298.5	62.4
303.0	34.3
307.7	18.5
312.5	9.8
317.5	5.0
322.5	2.49

Data analysis shows that solar radiation with the wavelengths shorter than 290 nm hardly reaches the earth's surface being absorbed in the upper

atmospheric layers. Therefore, Fig. 2 depicts the daily dynamics of solar radiation intensity in the spectral region of 292.5 to 320 nm.

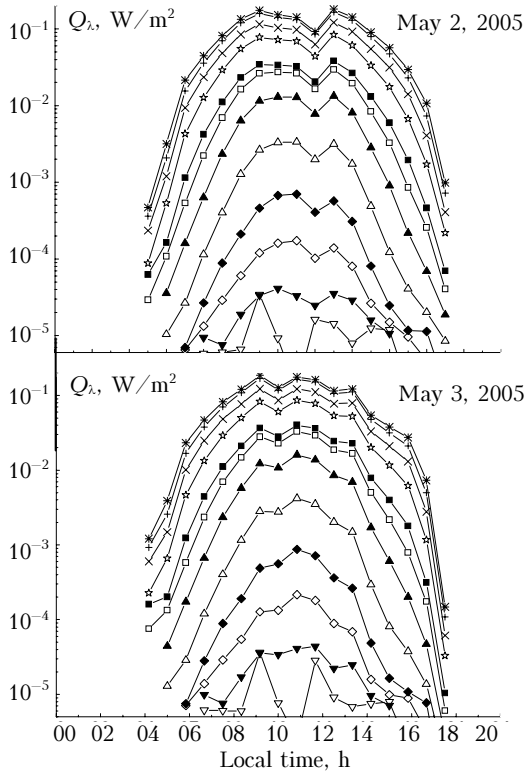

Fig. 2. Daily variations of UV-B radiation depending on the wavelength: (▽) 292.5 nm, (▼) 295, (◇) 297.5, (◆) 300, (△) 302.5, (▲) 305, (□) 307.5, (■) 310, (☆) 312.5, (✳) 315, (┼) 317.5, (✳) 320 nm.

From Fig. 2 we can see that the major part (> 90%) of the UV-B radiation has the wavelengths $\lambda > 310$ nm. However, the ozone absorption cross section at these wavelengths decreases by two orders of magnitude, and the quantum yield of metastable oxygen $O(^1D)$ drops down several times (Fig. 3).

Consequently, under certain conditions this may lead to a more or less uniform distribution of the photodissociation coefficients depending on the wavelength, which can be seen in Fig. 4*a*.

In the morning and evening hours, the values of J_λ in the wavelength region from 305 to 320 nm keep within approximately 1.0 to 10^{-7} s^{-1}. In the daytime, the major contribution to formation of metastable oxygen $O(^1D)$ comes from the radiation with the wavelengths 305 nm < λ < 310 nm, regardless of its weak intensity at the earth's surface. The integral values of J calculated by Eq. (38) with the account of the parameters measured at our TOR Station are given in Fig. 4*b*. The values of $J_{O(^1D)}$ obtained correspond to data presented in Refs. 1 and 6. Hence, they are applicable to calculation of the concentration of $O(^1D)$ and of hydroxyl radical.

From the calculated results on $O(^1D)$ and OH (Fig. 5) we can see that because of the dependence of the formation of these components on the UV-B radiation intensity, the obtained daily variation is plotted as a bell-shaped curve, which is close to the daily behavior of nanoparticle concentration, whose diameter does not exceed 10 nm. The values of the daytime $O(^1D)$ concentrations keep within $1 \cdot 10^{-3}$–$9 \cdot 10^{-3}$ cm^{-3}, and for OH within $1 \cdot 10^5$–$5 \cdot 10^5$ cm^{-3} being comparable with the experimental data.[1,6,9,14]

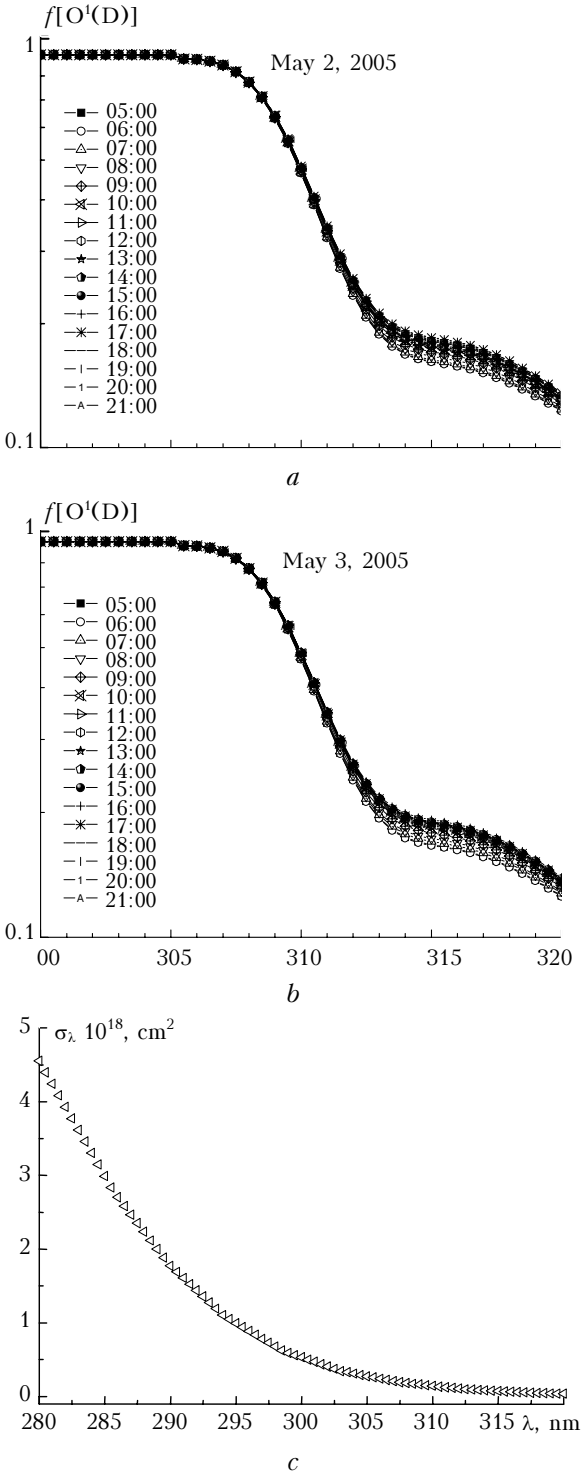

Fig. 3. Quantum yield of $O(^1D)$ under ozone photolysis (*a*, *b*) and ozone absorption cross section (*c*).

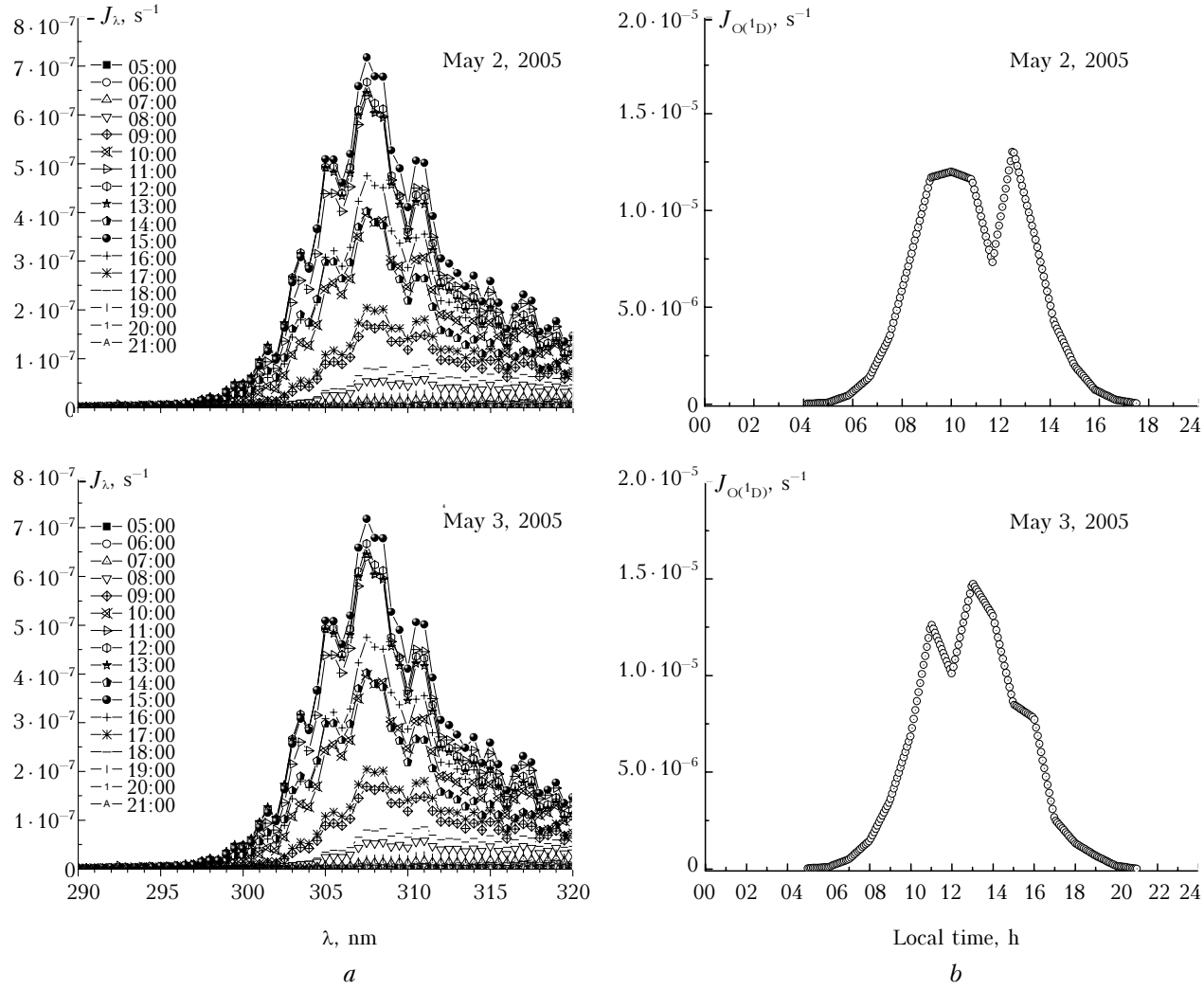

Fig. 4. Daily dynamics of ozone photodissociation coefficient depending on the wavelength (*a*) and irrespective of the wavelength (*b*).

3.3. Calculation of H_2SO_4 and HNO_3 concentrations. Estimate of nucleation rate

The stationary concentrations of sulfuric and nitric acids can be calculated as follows:

$$[H_2SO_4] = k_{11}[OH][SO_2]\tau, \quad (43)$$

$$[HNO_3] = k_{23}[OH][NO_2]\tau, \quad (44)$$

where τ is the heterogenic sink rate to aerosol particles that always exist in the atmosphere, (in time units). The quantity of the so-called heterogenic sink time τ was calculated using the expression from Refs. 9 and 15:

$$\tau = \left(4\pi D \int \frac{\bar{r}_p n(r_p)}{1 + a_c l / \bar{r}_p} dr_p \right)^{-1}, \quad (45)$$

where D and l are the diffusion coefficient and the free path of a condensing substance, respectively; a is the correction factor varying from 0.8 to 1.1; $n(r_p)$ is the size distribution of particle number concentration.

The time needed for establishing the stationary state between the formation and sink to the aerosol particles of condensing substances varied from $\approx 10^2$ to 10^3 s.

The concentrations of sulfuric and nitric acids calculated by Eqs. (43) and (44) are given in Fig. 6. As in the case of metastable oxygen and hydroxyl radical, the calculated values keep within the experimental concentration limits of H_2SO_4 and HNO_3.[1,6,7,9,14]

Before we turn to the particle formation and nucleation processes, we must determine if the amount of the initial substances contained in the atmosphere is sufficient for forming the aerosol mass we consider. To do this, we turn back to Eqs. (43) and (44). If we remove τ from their right-hand parts, we shall have the sulfuric and nitric acid formation rates (Fig. 7).

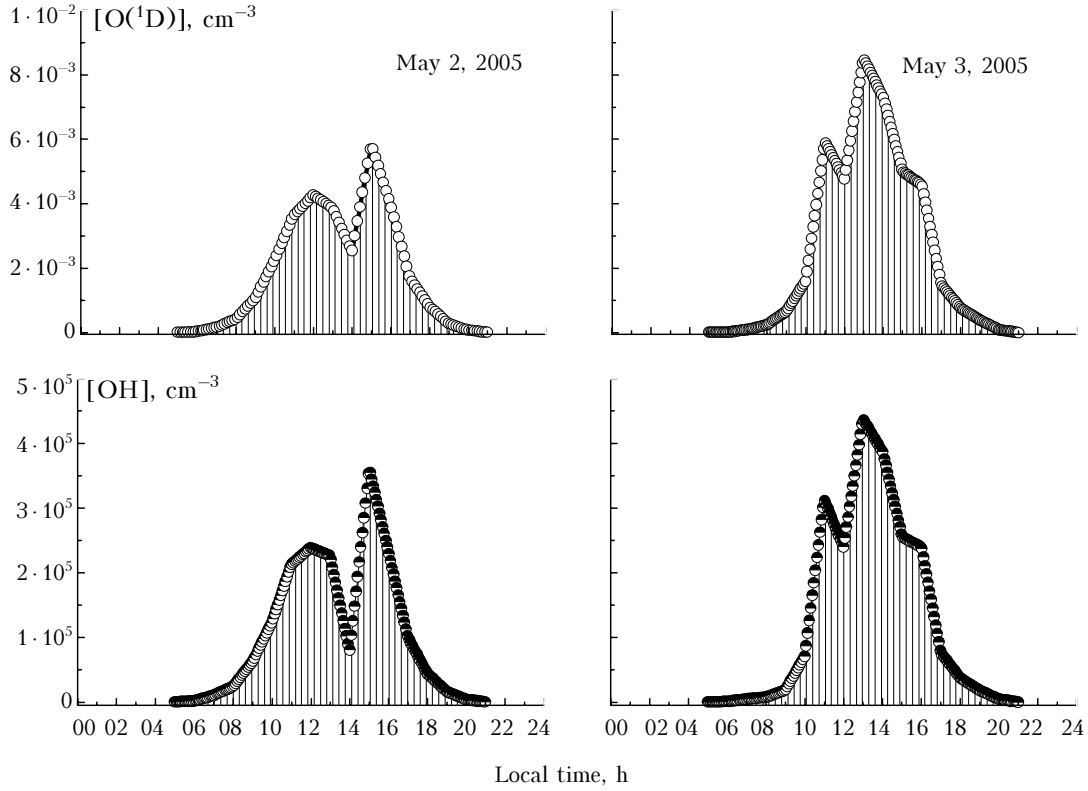

Fig. 5. Calculated stationary concentrations of metastable oxygen O(¹D) and hydroxyl radical OH.

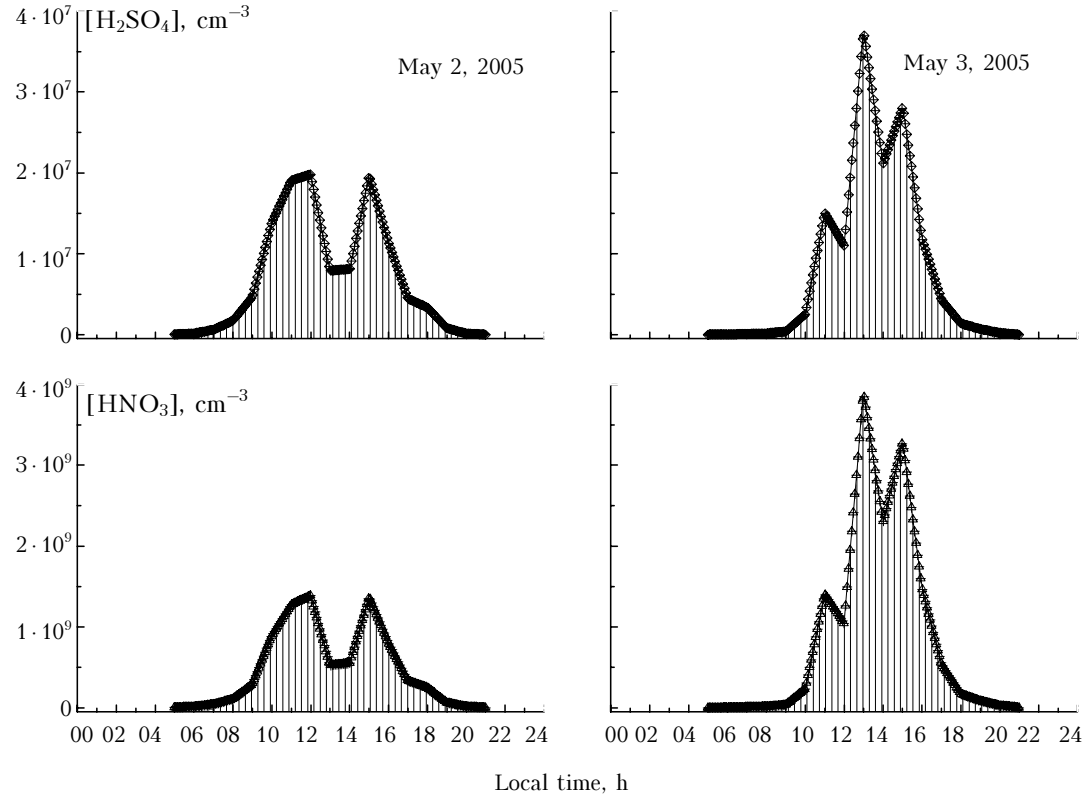

Fig. 6. Calculated stationary concentrations of sulfuric and nitric acids.

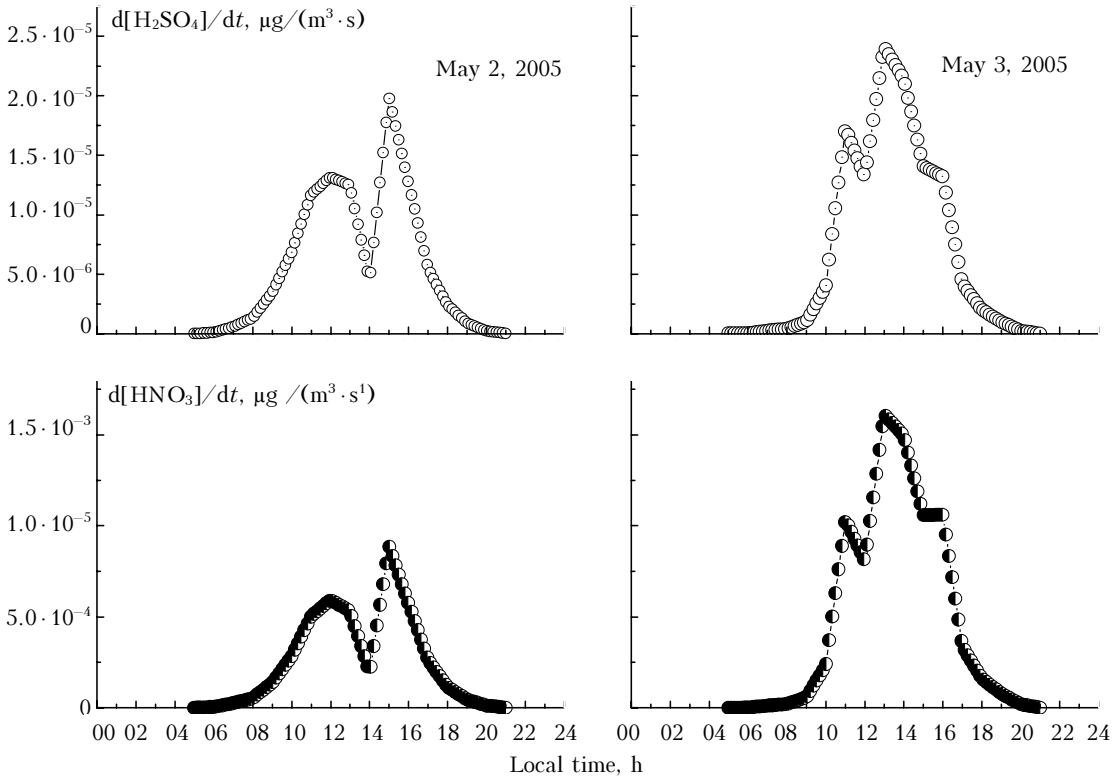

Fig. 7. Rates of sulfuric and nitric acid formation in the atmosphere.

By time-integration of the formation rates, we obtain the substance mass formed in a unit volume during the time period considered. As a result, we have that during daytime, the photochemical and gas-phase conversions in the atmosphere lead to formation of ≈0.3–0.5 μg/m^3 of sulfuric acid and of ≈15–30 μg/m^3 of nitric acid. As a postulate of aerosol thermodynamics reads, nearly the entire amount of sulfuric acid converts from gas to aerosol phase.[9]

The studies of the ion and elemental composition of aerosol performed over Siberia[6,15–19] demonstrate that in the surface layer, the weight ratio of sulfates is approx. 5–10.0 μg/m^3. Thus, the values obtained for sulfuric acid well agree with the data on ion composition of aerosol, if we take into account that the bulk aerosol weight is formed by particles of 0.1–1.0 μm size with an approximately ten-day lifetime.[20] The nitrate content in aerosol is much lower than the amount of the nitric acid that forms in the atmosphere. Apparently, the most of nitric acid is withdrawn from the atmosphere through gas-phase chemical sinks and dry and wet precipitation.[6,9] because of its high chemical reactivity and solubility.

In spite of the fact that all the above-described processes yield aerosol particles from the gas phase, the mechanism of homogeneous nucleation is still unclear.

It is yet impossible to measure the atmospheric nucleation rate directly, for there are still no methods available for detecting critical embryos, and in the methods available, the lower limit of the particle detection is 2.5–3.0 nm. For this reason, the so-called particle formation rate J_d is normally calculated, which is mathematically equal to the flux of particles with the size exceeding a certain value d due to condensation growth of the particles[21]:

$$J_d(t') = \left.\frac{\mathrm{d}n(d_\mathrm{p},t')}{\mathrm{d}d_\mathrm{p}}\right|_d \left.\frac{\mathrm{d}d_\mathrm{p}}{\mathrm{d}t'}\right|_d, \qquad (46)$$

where t' is the time; $n(d_\mathrm{p}, t)$ is the size distribution of particle number concentration.

Since the method of calculating the instantaneous $J_d(t')$ value is difficult either, a much wider application has gained another method, which consists in calculation of the average J_d over a chosen particle formation process time Δt (Refs. 3, 21, and 22):

$$\left.\frac{\Delta N_{d,d_\mathrm{max}}}{\Delta t'}\right|_\mathrm{observ} = J_d - \left.\frac{\Delta N_{d,d_\mathrm{max}}}{\Delta t'}\right|_\mathrm{self\text{-}coag.} - \left.\frac{\Delta N_{d,d_\mathrm{max}}}{\Delta t'}\right|_\mathrm{coag.} - \left.\frac{\Delta N_{d,d_\mathrm{max}}}{\Delta t'}\right|_\mathrm{transfer}, \qquad (47)$$

where N_{d,d_max} is the total number concentration of particles in the size range from d to d_max; d_max is the maximum size, which a particle can reach during the growth time Δt. The second and third terms in the right-hand part stand for the losses due to self-coagulation and coagulation on particles whose size exceeds d_max, the last component accounts for the losses due to transport of air masses. Under

conditions of expressed nucleation or, in our case, a sufficient rate of J_d, the second and third terms are negligibly small compared with J_d and therefore, can be ignored. A bell-shaped daily variation of ultrafine particle concentration is indicative of that the last right-hand term can also be ignored. According to M. Kulmala et al.,[21] Eq. (47) takes the form

$$J_{\mathrm{d}} \approx \left.\frac{\Delta N_{\mathrm{d},d_{\max}}}{\Delta t}\right|_{\mathrm{observ.}}. \qquad (48)$$

In order to determine $d_{\max}$, we must find the growth rate by the equation[14,16]

$$GR \approx \frac{d - d_{\mathrm{crit}}}{t'_{\mathrm{form}} - t'_{\mathrm{nucl}}}, \qquad (49)$$

where d_{crit} is the diameter of a critical embryo (cluster) that equals ~1 nm according to the nucleation theory; d is the diameter that corresponds to the detection limit of the measurement equipment (in our case it is 3 nm); t'_{nucl} is the nucleation start time, which is usually determined by the starting aerosol precursor concentration growth, for example, that of sulfuric acid; t'_{form} is the moment the concentration of 3 nm sized particles starts to grow.

Thus calculated growth rates are ≈ 1.5 nm/h. As a result, by the moment of highest ultrafine particle concentration, the cluster sizes are within the range of $d_{\mathrm{p}} \approx 10$ nm. Hence, in Eq. (48) we can take this size for $d_{\max}$.

In this connection, $J_{10\,\mathrm{nm}} = 0.45$ (May 2, 2005) and 0.34 $\mathrm{cm^{-3} \cdot s^{-1}}$ (May 3, 2005).

However, after the sunset, when J_d must be close to zero because of a critical fall of the concentration of the main aerosol precursors, a decrease in the concentration of $d_{\mathrm{p}} < 10$ nm particles takes some time to reach minimum value. Therefore, our $J_{10\,\mathrm{nm}}$ is a bit underestimated, because in Eq. (48) we did not manage to take into account variation in these particles concentration due to coagulation. Although the coagulation rate is not that high, it acts all the time. And after the moment when the grown particles have reached 10 nm in diameter, we must take into account variations in the concentrations of this size particles as well. The total of these losses can be estimated by the delay of the concentration decrease after the supposed termination of the nucleation. The rate of these losses was ≈0.055 $\mathrm{cm^{-3} \cdot s^{-1}}$. Thus, with the allowance for this correction $J_{10\,\mathrm{nm}} \approx 0.4$–$0.5$ $\mathrm{cm^{-3} \cdot s^{-1}}$.

Now, let us compare our value with the theoretical rate of the binary nucleation of water and sulfuric acid. For the calculation, we used the empirical equation proposed by K. Capaldo[23] and based on the classical theory of homogeneous nucleation:

$$\log J = -(64.24 + 4.7f) + (6.13 + 1.95f) \times \times (\log[\mathrm{H_2SO_4}] + (298 - T)/25). \qquad (50)$$

Thus calculated results clearly (Fig. 8) prove that the binary nucleation of H_2O and H_2SO_4 cannot guarantee formation of nanoparticles in the amount observed, at least in the surface atmospheric layer. The rate of critical embryo formation must exceed that of particle concentration growth, because most embryos are not quick enough to reach 3 nm in size due to heterogeneous condensation onto the available aerosol particles.

However, the circumstance that the nucleation rates calculated for May 3, 2005 are lower than those calculated for May 2, 2005, is indicative of that we have chosen the right way, for the concentration of ultrafine particles on May 3 was also lower. Most likely, in the near-surface layer, there prevails a three-component nucleation of sulfuric acid, ammonia, and water.

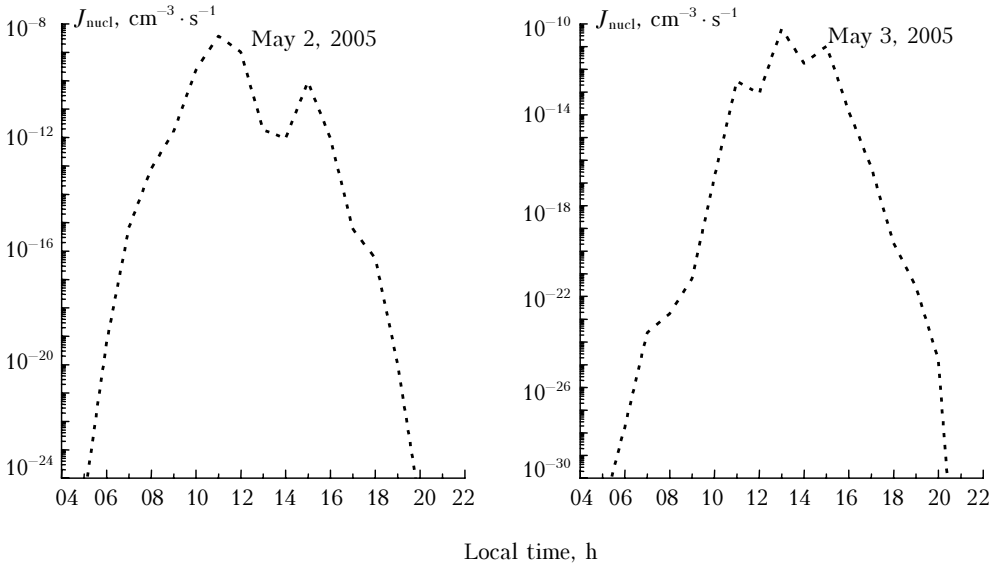

Fig. 8. The model rate of a binary homogeneous nucleation for sulfuric acid and water.

According to I. Napari et al.,[24] the presence of even a small amount of NH_3 raises the nucleation rate by several orders of magnitude. For example, their calculations showed that as little as 0.04 ppb of NH_3 in the presence of $H_2SO_4 \approx 10^7$ cm^{-3} increases the rate up to 10^1 cm$^{-3}\cdot$s^{-1} (at $T = 298.15$ K and a 50% relative humidity). Here, according to J. Seinfeld[9] in the continental atmosphere the concentration of ammonia varies within 0.1–10.0 ppb.

It is more likely that nitric acid, along with some highly volatile organic compounds, participates in the heterogeneous condensation processes than in the homogeneous nucleation. For example, I. Napari et al.[25] in their calculations have demonstrated that to reach any significant nucleation rates for different variations of three-component homogeneous nucleation that involve nitric acid, the concentration of the latter must be at least $\approx 10^{16}$–10^{18} cm^{-3}, which is impossible in real earth's atmosphere. However, today, the binary homogeneous nucleation of the system HNO_3–H_2O attracts more and more attention in the context of the problem of formation of polar stratospheric clouds. Most authors believe that the probability of this process is low because the pressure of the saturated vapor of nitric acid is much higher than that of sulfuric acid, thus HNO_3 is captured by the molecules of H_2SO_4–H_2O forming the particles of a three-component solution. A four-component nucleation (H^+–NH_4^+–SO_4^{2-}–NO_3^-–H_2O) is also possible, but the thermodynamics of this process is so complex that the results obtained by different researchers vary too much.

Since we did not aim at going deeply into the nucleation process in this paper, we shall give a thorough consideration of all the possible variants of the nucleation processes in a series of works devoted to the atmospheric gas-to-particle conversion.

In the upper troposphere and lower stratosphere, a binary homogeneous nucleation of sulfuric acid and water can play one of the key roles, for its rate strongly depends on temperature: if the temperature decreases, its rate jumps up by orders of magnitude. At the same time the role of the three-component nucleation that involves ammonia becomes less important, for the concentration of ammonia in the upper atmospheric layers is negligibly low.

Summary

Continuous measurements of nanoparticles performed in the 2005 with a better time resolution than in previous investigations have proved an expressed daily behavior of the concentration of ultrafine particles first observed in 1996.

A bell-shaped daily behavior results from the photochemical formation of aerosol precursors. The photochemical processes yielding sulfate and nitrate aerosols from the gas phase are initiated in the surface layer mainly by the UV radiation of 305–310 nm wavelength.

The estimate of the nanoparticle formation rate performed by the method different from the one we used previously, has given somewhat larger values, though the order of magnitude is the same.

Calculations of the concentrations of the main aerosol gas precursors, where we used the UV-B radiation measurement data, meteorological information, and the values of ozone concentration and of some greenhouse gases obtained at the IAO TOR Station, gave quite reliable results comparable to the real atmospheric values. All this favors further uses of this approach for more detailed studies of the atmospheric nucleation processes.

Acknowledgments

The authors would like to acknowledge G.I. Skubnevskaya for the friendly and pertinent remarks she expressed at the Young Scientists School on the Environmental Physics, 2002, which made us to critically revise all the previous results.

The work has been done under the Programs 24.3.3 of the SB RAS and 13.4 of the RAS Presidium, and is supported by the Russian Foundation for Basic Research (Nos. 04–05–64559, 04–05–65179 and 04–05–08010).

References

1. C.D. O'Dowd, K. Hämeri, J.M. Mäkelä, L. Pirjola, M. Kulmala, S.G. Jennings, H. Berresheim, H.C. Hansson, G. de Leeuw, G.J. Kunz, A.G. Allen, C.N. Hewitt, A. Jackson, Y. Viisanen, and T. Hoffman, J. Geophys. Res. D**107**, No. 19, 8108, doi:10.1029/2001JD000555 (2002).
2. G.V. Rozenberg, Izv. Akad. Nauk USSR, Fiz. Atmos. Okeana **19**, No. 1, 21–35 (1983).
3. M.Yu. Arshinov and B.D. Belan, Atmos. Oceanic Opt. **13**, No. 11, 909–916 (2000).
4. H. Okabe, *Photochemistry of Small-sized Molecules* [Russian translation] (Mir, Moscow, 1981), 500 pp.
5. S.N. Dubtsov, E.N. Dultsev, G.I. Skubnevskaya, A.I. Levykin, and K.K. Sabelfeld, Atmos. Oceanic Opt. **18**, Nos. 5–6, 363–366 (2005).
6. V.A. Isidorov, *Ecological Chemistry* (Khimizdat, St. Petersburg, 2001), 304 pp.
7. Yu.A. Israel, I.M. Nazarov, and A.Ya. Pressman, *Acid Rains* (Gidrometeoizdat, Leningrad, 1983), 206 pp.
8. R. Atkinson, D.L. Baulch, R.A. Cox, J.N. Crowly, R.F. Hampson, R.G. Hynes, M.E. Jenkin, M.J. Rossi, and J. Troe, Atmos. Chem. Phys., No. 4, 1461–1738 (2004).
9. J.H. Seinfeld and S.N. Pandis, *Atmospheric Chemistry and Physics: from Air Pollution to Climate Change* (Wiley and Sons, New York, 1998), 1327 pp.
10. M.Yu. Arshinov, B.D. Belan, D.K. Davydov, V.K. Kovalevsky, A.P. Plotnikov, E.V. Pokrovsky, and G.N. Tolmachev, Meteorol. Gidrol., No. 3, 110–118 (1999).
11. G.P. Reischl, A. Majerowicz, A. Ankilov, S. Eremenko, and R. Mavliev, J. Aerosol Sci. **22**, No. 2, 223–228 (1991).
12. E.O. Knutson, Aerosol Sci. Technol. **31**, 83–128 (1999).
13. M.Yu. Arshinov, B.D. Belan, and T.K. Sklyadneva, in: *Proc. of EUROTRAC Symp. 98* (WJT Press, Sauthampton, 1999), Vol. 1, pp. 495–500.

14. R.J. Weber, J.J. Marti, and P.H. McMurry, J. Geophys. Res. D**102**, No. 4, 4375–4385 (1997).
15. A.S. Kozlov, A.N. Ankilov, A.M. Baklanov, A.L. Vlasenko, S.I. Eremenko, S.B. Malyshkin, and S.E. Peshchenko, Atmos. Oceanic Opt. **12**, No. 12, 1046–1052 (1999).
16. B.D. Belan, D.V. Simonenkov, and G.N. Tolmachev, Proc. SPIE **5026**, 407–410 (2002).
17. B.S. Smolyakov, K.P. Koutsenogii, L.P. Osipova, V.F. Raputa, L.A. Pavlyuk, and S.M. Filimonova, Atmos. Oceanic Opt. **13**, Nos. 6–7, 565–569 (2000).
18. B.S. Smolyakov and M.P. Shinkorenko Atmos. Oceanic Opt. **15**, Nos. 5–6, 397–400 (2002).
19. A.N. Ankilov, A.M. Baklanov, A.S. Kozlov, and S.B. Malyshkin, Atmos. Oceanic Opt. **13**, Nos. 6–7, 597–601 (2000).
20. B.D. Belan, A.I. Grishin, G.G. Matvienko, and I.V. Samokhvalov, *Spatial Variability of Aerosol Characteristics* (Nauka, Novosibirsk, 1989), 152 pp.
21. M. Kulmala, H. Vehkamäki, T. Petäjä, M. Dal Maso, A. Lauri, M.-M. Kerminen, W. Birmili, and P.H. McMury, J. Aerosol Sci. **35** No. 2, 143–176 (2004).
22. M. Dal Maso, M. Kulmala, J. Mäkelä, L. Pirjola, and A. Laaksonen, Report Series in Aerosol Sci., No. 47, 23–32 (2000).
23. K. Capaldo, P. Kashibhatla, and S.N. Pandis, J. Geophys. Res., No. 104, 3483–3500 (1999).
24. I. Napari, M. Noppel, H. Vehkamäki, and M. Kulmala, J. Chem. Phys. **116**, No. 10, 4221–4227 (2002).
25. I. Napari, M. Kulmala, and H. Vehkamäki, J. Chem. Phys. **117**, No. 18, 8418–8425 (2002).